Neuron, Volume *81*

Supplemental Information

Pharmacological Correction of Gating Defects in the Voltage-Gated $Ca_V2.1$ Ca^{2+} Channel due to a Familial Hemiplegic Migraine Mutation

Akira Inagaki, C. Andrew Frank, Yuriy M. Usachev, Morris Benveniste, and Amy Lee

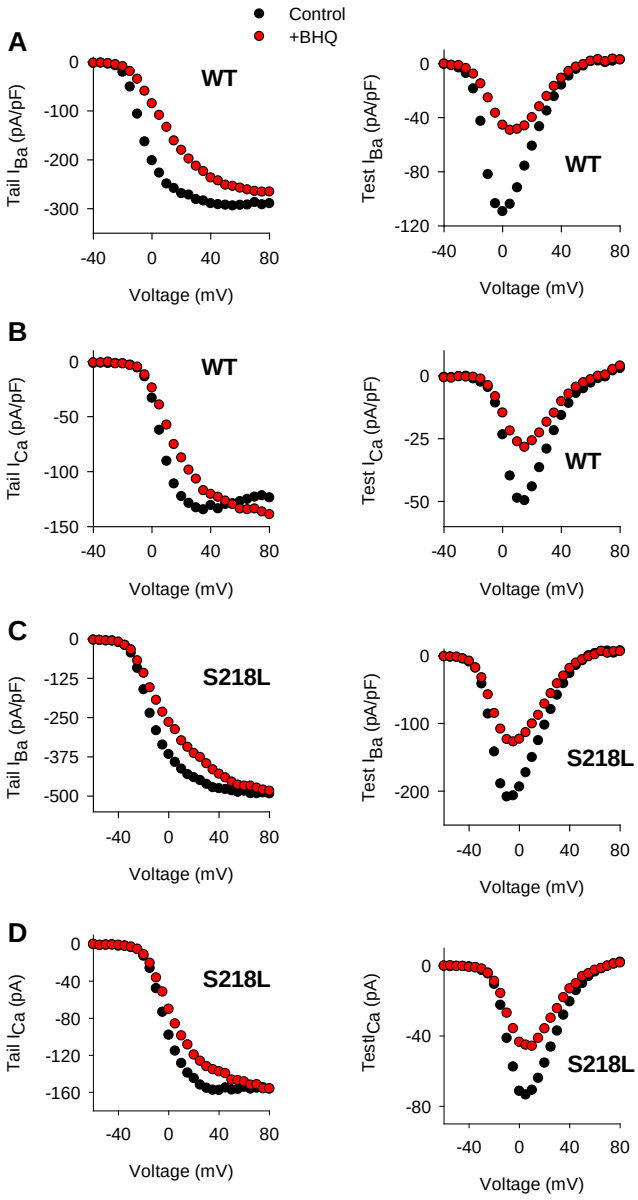

Figure S1 related to Fig.1. **BHQ inhibits voltage-dependent activation of WT and S218L.** Voltage protocols involved step depolarizations to various voltages from a holding voltage of -80 mV and were the same as in Fig.1E,F and I,J of the main text. Each graph shows current density for tail currents recorded upon repolarization (left) or test currents (during the depolarizing step, right). Recordings of tail and test currents were done on a single cell (different cells in A-D) using Ba^{2+} (A,C) or Ca^{2+} (B,D) as the charge carrier. BHQ did not affect the maximal tail current amplitudes obtained at +85 mV, arguing against an open-channel blocking mechanism. In addition, the magnitude of test current inhibition corresponded to the degree of inhibition of the voltage-dependence of activation. Together, these results suggest that inhibition of voltage-dependence of activation by BHQ largely accounts for the inhibition of the steady-state current.

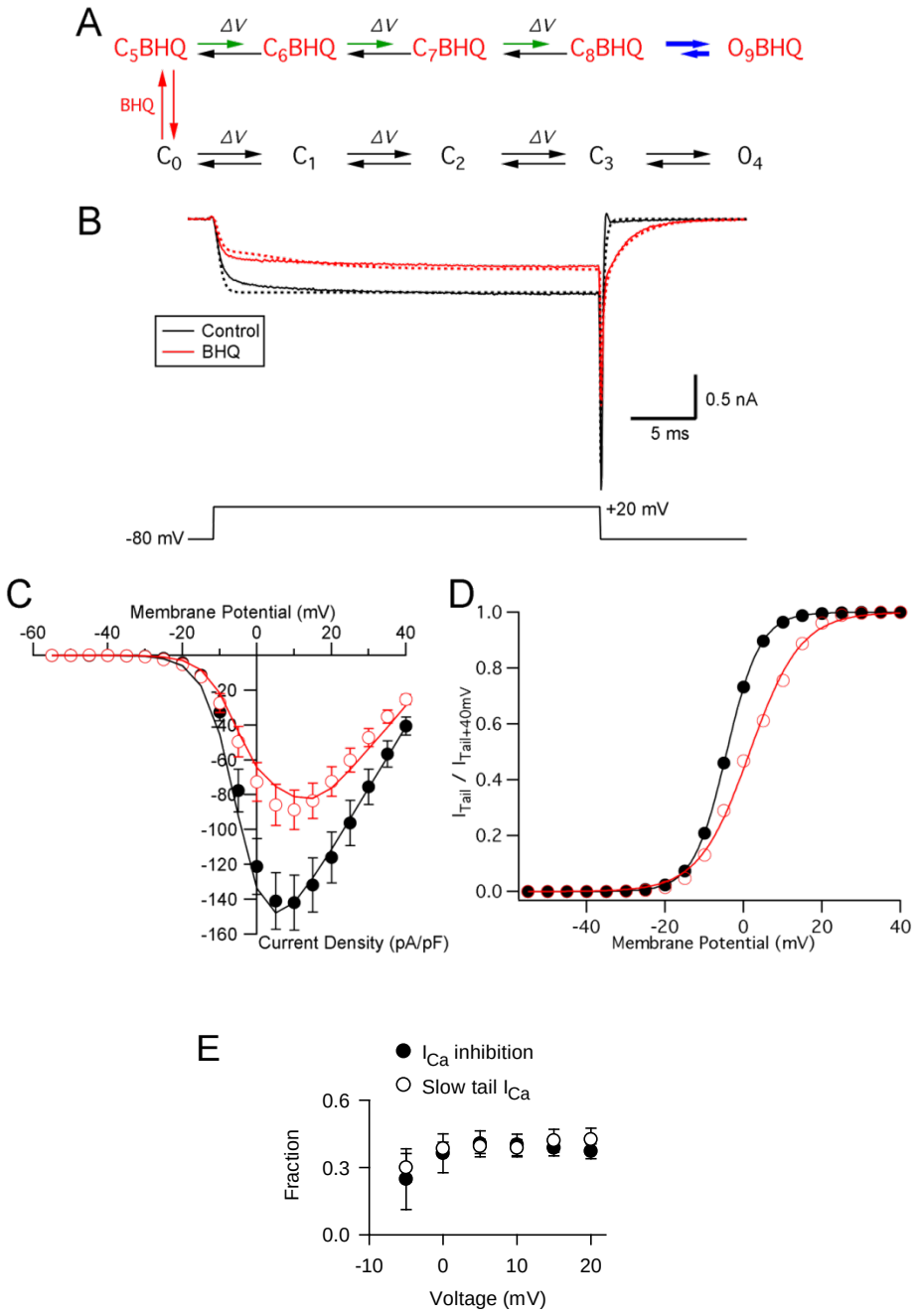

Figure S2 related to Fig.3. **Slowing of voltage-independent deactivation and voltage-dependent activation is required to simulate effects of BHQ on $Ca_v2.1$ currents.** ***A***. 10-state model used to predict the effects of BHQ. Because our experiments were done with a subsaturating level of BHQ, we developed a model with two populations of channels, those modulated by BHQ (red) and those not modulated by BHQ (black). Although BHQ may regulate multiple activation states of the channel, we assumed that BHQ-modulated channels were in equilibrium at the beginning of the simulated trace. We also assumed a K_d for BHQ of 5 µM, and the concentration of BHQ utilized in these simulations was 10

μM. Finally, we also assumed that control and BHQ-modulated open states (O_4 and O_9BHQ, respectively) have the same conductance. Colored transitions indicate rates that differ from control conditions without BHQ. *ΔV* indicates voltage-dependent transitions. ***B***. Ca^{2+} currents (I_{Ca}) recorded in a HEK293T cell transfected with $Ca_v2.1$ channels (solid lines) during a voltage-clamp experiment, and fitted, simulated currents (dotted lines) generated by the model in *A*. Fitting was performed simultaneously on entire family of leak-subtracted traces in the presence and absence of 10 μM BHQ (20 traces of control, 20 traces in BHQ). The voltage range for evoked currents was from -55 mV to +40 mV in 5 mV increments, with a holding potential of -80 mV. Fits were limited to voltage steps with an upper limit of +40 mV, because our model could not predict the curvilinear region of the points approaching the reversal potential. Shown are actual and simulated traces for voltage steps to +20 mV. Although fits approximate real data, deviations may be due to the fact that this model does not simulate Ca^{2+}- dependent facilitation. Ca^{2+} rather than Ba^{2+} currents were used because the slowing of deactivation was greater and easier to measure. Simulations were also done for Ba^{2+} currents (data not shown), with generally similar results for the effects of BHQ. Basic features of the data reproduced by the model are: 1) slowing of the tail current in the presence of BHQ; 2) inhibition of the steady state current in the presence of BHQ (***C***); and 3) shift in the voltage dependence of the tail current (***D***). ***C***. Steady state current-voltage relationship for experimental and simulated I_{Ca}. Circles (black, Control; red, 10 μM BHQ) represent the steady state averaged (±SEM) I_{Ca} density experimentally obtained with the voltage protocol in ***B*** (n = 11 cells for both control and BHQ). Smooth lines are the simulated I_{Ca} steady-state density utilizing the parameters determined from fits of experimental data in *B*. Simulated amplitudes were normalized to the maximum current density of control (at a membrane potential of +10 mV). ***D***. Normalized tail current-voltage relationship for the simulated peak tail currents (control, black circles; 10 μM BHQ, red circles) generated upon repolarization to -80 mV from varying test voltages. The simulated currents were generated with parameters from data obtained in *B* and normalized to the simulated peak tail current obtained at +40 mV. Fitting with the Boltzmann equation yielded the following parameters: Control: $V_{1/2}$ = -4.3 mV, k = 4.3; 10 μM BHQ: $V_{1/2}$ = +1.6 mV, k = 6.5. Comparison of the fits between control and BHQ simulated data showed a similar trend in the increase in both $V_{1/2}$ and slope (k) albeit different magnitudes from the experimental data (Control: $V_{1/2}$ = -1.9 mV, k = 6.0; 10 μM BHQ: $V_{1/2}$ = +6.8 mV, k = 9.0). These differences may be attributed to the simplicity of the model and limiting the number of parameters utilized in the fit (*see below*). ***E***, Experimental data showing equivalence between the fraction of test pulse-evoked I_{Ca} that is inhibited by BHQ and the fraction of the slow component of the tail current. Fractional inhibition of I_{Ca} amplitude (filled circles) by BHQ was determined from *I-V* data obtained in Fig.3A of the main text. The slow tail I_{Ca} (open circles) represents the fraction of the slow component of deactivation that was measured from double exponential fits of the tail I_{Ca} decay. Both were plotted against test voltage. n=7 cells.

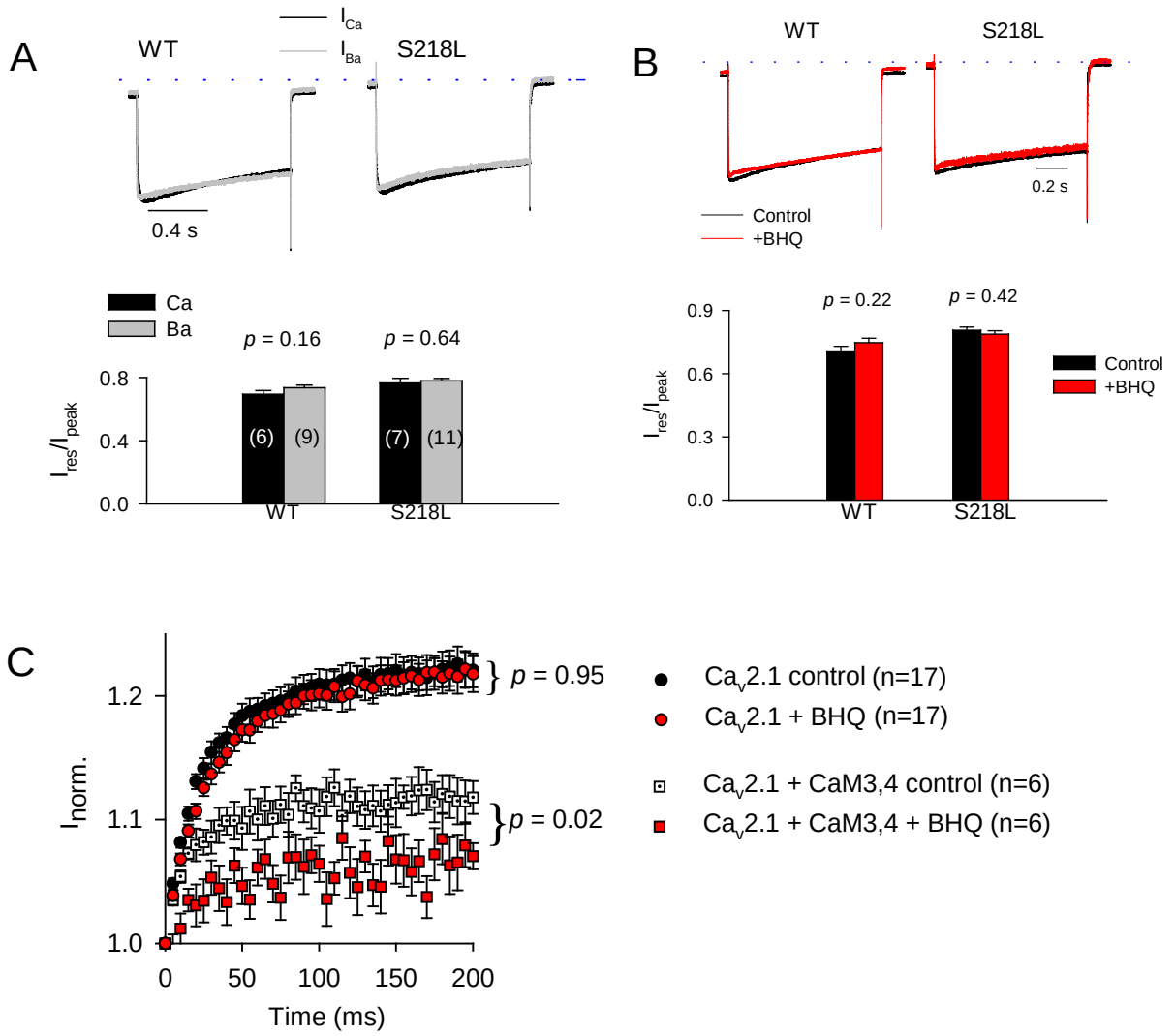

Figure S3 related to Fig.4. Effect of BHQ on CDF is not secondary to an effect on inactivation but does require Ca^{2+}/ CaM. (A) Intracellular EGTA (5 mM) is sufficient to block Ca^{2+}-dependent inactivation (CDI). I_{Ca} was evoked by 1-s pulses to +10 mV from -80 mV in HEK293T cells transfected with wild-type (WT) $Ca_v2.1$ or S218L mutant. Representative traces are shown (I_{Ca} is largely obscured by I_{Ba} for S218L). Inactivation was measured as the ratio of the residual current amplitude at the end of the pulse and the peak current amplitude (I_{res}/I_{peak}). Parentheses indicate numbers of cells. (B) BHQ does not affect voltage-dependent inactivation. I_{Ba} was evoked by 1-s pulses to +10 mV from -80 mV before (control, black) and after exposure to 10 μM BHQ (+BHQ, red) in cells transfected with $Ca_v2.1$ (WT or S218L). Representative traces are shown (control trace is largely obscured by +BHQ trace for S218L). For WT, n= 6, and for S218L, n=5. In *A* and *B*, values shown in the bar graph represent mean ± SEM; p-values were determined by t-test. (C) Effects of BHQ on I_{Ca} during APW trains require CaM-dependent CDF. Same protocol as in Fig.4 of main article. Results for I_{Ca} are shown. Cells were transfected with $Ca_v2.1$ alone or cotransfected with calmodulin mutant that cannot bind Ca^{2+} in the C-terminal EF-hands (CaM3,4). This mutant is unable to transduce CDF for $Ca_v2.1$ channels, such that residual facilitation of I_{Ca} represents primarily VDF. The effects of BHQ on enhancing CDF of $Ca_v2.1$ are evident in the maintained facilitation of I_{Ca} in cells transfected with $Ca_v2.1$ alone, despite inhibition of VDF (see

Fig.4E). The effects of BHQ in inhibiting VDF are shown by the significantly weaker facilitation of I_{Ca} in the presence of BHQ in cells cotransfected with CaM3,4. P-values were determined by t-test.

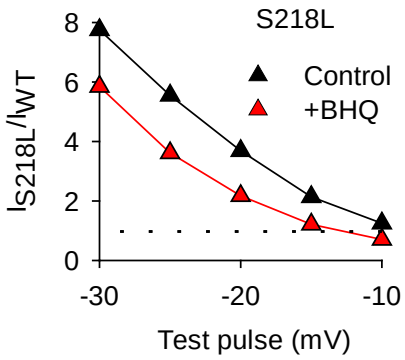

Figure S4 related to Fig.5. BHQ reduces gain of function of S218L. Gain-of function due to the S218L mutation was expressed as the ratio of mean I_{Ba} amplitude for WT (Fig.1E) and S218L (Fig.5D) (I_{S218L}/I_{WT}) under control conditions and with BHQ. Values were plotted against test voltage. Dashed line indicates equivalence between WT and S218L amplitudes (ratio=1).

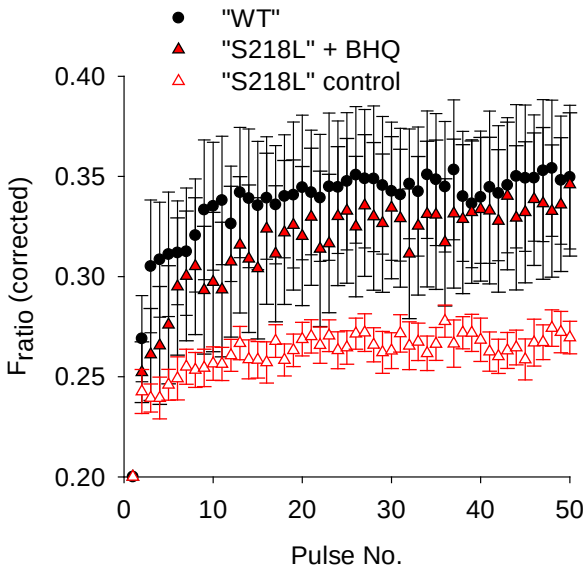

Figure S5 related to Fig.9. The effects of BHQ on STF are independent of effects of BHQ on the Ca^{2+} cooperativity of neurotransmitter release in "S218L". mEPSP and EPSP data were obtained as in Fig. 8, except that extracellular solution contained 0.2 mM Ca^{2+}. From these data, quantal contents (QC) were calculated and then corrected for non-linear summation (NLS QC) (as in (Martin, 1955)).To determine Ca^{2+} cooperativity of transmitter release, NLS QC was plotted on a log-log scale against extracellular [Ca^{2+}] to determine a slope value for each experimental condition (2.65 for "WT", 2.61 for "S218L", and 3.21 for "S218L" + BHQ). Since BHQ increases Ca^{2+} cooperativity of "S218L", it was possible that effects of BHQ on STF were not due solely to effects on CDF. Therefore, we used the slope values obtained from the Ca^{2+} cooperativity plots to obtain F_{ratio} (corrected) for each pulse during the 10 Hz train, which took into account effects of BHQ on Ca^{2+} cooperativity. Plotting these values against pulse number revealed a significant difference in F_{ratio} (corrected) between "WT" and "S218L" ($p < 0.05$ at pulse 50, by Student's t-Test), despite their nearly identical Ca^{2+} cooperativity slopes. By contrast, there is no difference in F_{ratio} (corrected) between "WT" and "S218L" + BHQ ($p = 0.95$ at pulse 50, t-test), indicating a restoration of STF in the "S218L" mutant cannot be explained simply by an increase in Ca^{2+} cooperativity, but more likely a restoration of CDF.

Supplemental Experimental Procedures

Modeling**:**

Discussion of Model Parameters – General Considerations: The goal of this modeling study was to determine potential modes of action of BHQ on $Ca_v2.1$ activation and deactivation without consideration for complicating processes such as Ca^{2+}/CaM-dependent inactivation and facilitation. Although there are 30 rate parameters and the number of channels which can vary in this model, we simplified the number of needed parameters by assuming standard macroscopic multipliers for the voltage-independent components of the microscopic rate constants. Also, to reduce the number of parameters, we assumed symmetry in the voltage dependence of the forward and reverse rate constants. Ca_v channels are commonly modeled with 3 voltage dependent transitions and one voltage independent transition. Simulation of voltage-dependent transitions with the voltage-dependent component remaining constant for all three voltage-dependent transitions resulted in simulated currents that yielded an activation curve that was either too steep or too shallow. Thus, we allowed the voltage-dependent component to vary for all three voltage dependent transitions. Indeed, successful simulation of currents showed little voltage dependence for the first two transitions in the activation process.

Model Rate Constants:

Transition	Voltage Independent Forward Rate Constant	Voltage Independent Reverse Rate Constant	Voltage Dependence of Forward Rate Constant	Voltage Dependence of Reverse Rate Constant
C_0 <--> C_1	3*1244 s^{-1}	250 s^{-1}	-50 mV/*e*-fold	50 mV/*e*-fold
C_1 <--> C_2	2*1244 s^{-1}	2*250 s^{-1}	-40 mV/*e*-fold	40 mV/*e*-fold
C_2 <--> C_3	**1244 s^{-1}**	3*250 s^{-1}	-9 mV/*e*-fold	9 mV/*e*-fold
C_3 <--> O_4	5000 s^{-1}	5000 s^{-1}	--	--
C_5BHQ <--> C_6BHQ	3*130.2 s^{-1}	250 s^{-1}	-50 mV/*e*-fold	50 mV/*e*-fold
C_6BHQ <--> C_7BHQ	2*130.2 s^{-1}	2*250 s^{-1}	-40 mV/*e*-fold	40 mV/*e*-fold
C_7BHQ <--> C_8BHQ	**130.2 s^{-1}**	3*250 s^{-1}	-9 mV/*e*-fold	9 mV/*e*-fold
C_8BHQ <--> O_9BHQ	**154.9 s^{-1}**	**504.4 s^{-1}**	--	--
C_0 <--> C_5BHQ	1 $\mu M^{-1}s^{-1}$	5	--	--

-- indicates rate constants are not voltage dependent
Bolded values were those that varied during the fitting of the raw data traces

Determination of Specific Rate Constants – The aim of the modeling was to change the least number of rate constants to reproduce the behavior of BHQ. One critical characteristic of the action of BHQ is the slowing of deactivation. Following a number of simulations in which one or more rate constants were altered, it was determined that decreasing the rate constant of the transition from the open state to the last closed state (C_8BHQ <--O_9BHQ) was the only way to slow deactivation with this model. However, slowing this rate constant (504.4 s^{-1} *in the above table*) alone also yields a concomitant increase in steady state current, which is not observed in the real data. Therefore, we deduced that one of the

transitions leading to channel activation must also be reduced. To accomplish this, we simultaneously fit families of raw I_{Ca} traces in the presence and absence of BHQ. Since all traces of a dataset were acquired within a single cell, we assumed that the number of channels for both control and BHQ sets of data were the same (i.e., there was little or no rundown). Because of the large number of traces fit with varying voltage in the presence or absence of BHQ, fits with unique parameters could be found while varying 4 parameters (noted in bold in the table) and the number of channels. Thus, we could allow voltage-dependent and -independent forward rate constants to vary. We set the forward and reverse rate constant for channel opening and closing in the absence of BHQ arbitrarily (C_3 <-->O_4; 5000 s^{-1} and 5000 s^{-1}, respectively) since we have no information about those constants.

The parameters determined in the fit may be different if the parameters held constant were changed to other values. Based on extensive trials, we believe that the general trends of the parameters when comparing rate constants in the presence and absence of BHQ will remain similar. We tried to get good fits to the data by only varying the forward and reverse rate constants closest to the open state (C_8BHQ <--> O_9BHQ). This yielded reasonably good fits to the data. However, there was no difference between the voltage dependence of the peak amplitude of the tail current in the presence and absence of BHQ (Figure S3D). Next, we allowed the forward rate constant of the voltage dependent transitions (ie. C_5BHQ -->C_6BHQ) to vary in addition to the rate constant from the open state to the last closed state (C_8BHQ <-- O_9BHQ), with the forward rate constant to the open state (C_8BHQ --> O_9BHQ) set to 5000 s^{-1}. This yielded an abnormally wide current voltage relationship that did not match the data. Finally, when allowing both the forward rate constant of the voltage dependent (ie. C_5BHQ -->C_6BHQ) and independent (C_8BHQ --> O_9BHQ) transitions to vary in addition to the transition from the open state to the last closed state (C_8BHQ <-- O_9BHQ), the graphs in Figure S1 were obtained. Thus, the minimum number of changes required to produce BHQ like behavior are: 1) slowing of both the forward and reverse rate constants to and from the open state; and 2) slowing of the forward voltage dependent rate constant.

General Methods for Simulations – All simulations of currents under voltage clamp were performed using code originally written by John Clements (Benveniste et al., 1990), extensively modified and converted by M.B. to an Igor Pro XOP. Receptor state occupancies were determined numerically utilizing first order reaction kinetics as detailed in Benveniste *et al.* (1990). This was done iteratively at least 20 times per time point.

Supplemental References

Benveniste, M., Clements, J., Vyklicky, L., Jr., and Mayer, M.L. (1990). A kinetic analysis of the modulation of N-methyl-D-aspartic acid receptors by glycine in mouse cultured hippocampal neurones. J Physiol 428, 333-357.

Martin, A.R. (1955). A further study of the statistical composition on the end-plate potential. J Physiol 130, 114-122.